NANO LETTERS

Letter

pubs.acs.org/NanoLett

Thermal Management in Nanofiber-Based Face Mask

Ankun Yang,[†] Lili Cai,[†] Rufan Zhang,[†] Jiangyan Wang,[†] Po-Chun Hsu,[‡] Hongxia Wang,[†] Guangmin Zhou,[†] Jinwei Xu,[†] and Yi Cui*[,†,§]

[†]Department of Materials Science and Engineering and [‡]Department of Mechanical Engineering, Stanford University, Stanford, California 94305, United States

[§]Stanford Institute for Materials and Energy Sciences, SLAC National Accelerator Laboratory, 2575 Sand Hill Road, Menlo Park, California 94025, United States

Supporting Information

ABSTRACT: Face masks are widely used to filter airborne pollutants, especially when particulate matter (PM) pollution has become a serious concern to public health. Here, the concept of thermal management is introduced into face masks for the first time to enhance the thermal comfort of the user. A system of nanofiber on nanoporous polyethylene (fiber/nanoPE) is developed where the nanofibers with strong PM adhesion ensure high PM capture efficiency (99.6% for $PM_{2.5}$) with low pressure drop and the nanoPE substrate with high-infrared (IR) transparency (92.1%, weighted based on human body radiation) results in effective radiative cooling. We further demonstrate that by coating nanoPE with a layer of Ag, the fiber/Ag/nanoPE mask shows a high IR reflectance (87.0%) and can be used for warming purposes. These multifunctional face mask designs can be explored for both outdoor and indoor applications to protect people from PM pollutants and simultaneously achieve personal thermal comfort.

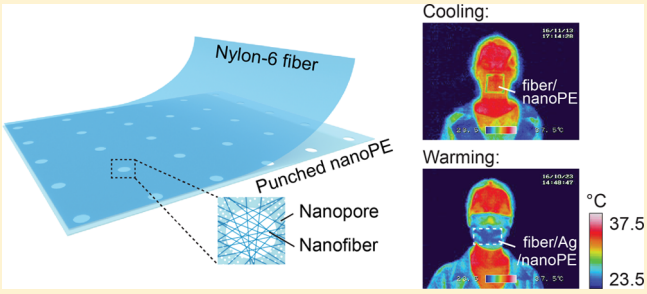

KEYWORDS: *Thermal management, nanofiber, face mask, filter, particulate matter*

Air pollution and climate change are two complex environmental problems caused by human activities, both related to large consumption of fossil fuels.[1−3] One of the major airborne pollutants, particulate matter (PM), has raised serious concerns in recent years.[4−6] PM is categorized by the particle size as $PM_{2.5}$ and PM_{10}, referring to PM with particle size below 2.5 and 10 μm, respectively. $PM_{2.5}$ with small particle sizes can penetrate bronchi and lungs and poses a severe health threat to the public.[6−8] To filter airborne pollutants, face masks have been widely used as safety equipment.[9] Commercial face masks are usually made of many layers of fibers (μm-size in diameter) and capture PM particles by a combination of physical barriers and adhesion.[10] To achieve a high PM removal efficiency, these face masks need to be thick and hence are often bulky and resistant to air flow (featured by a large pressure drop ΔP across the face mask). Consequently, breathing through these face masks can be uncomfortable or even dangerous for elderly people and people with lung diseases.[11] Nanofibers with large surface area-to-volume ratio have shown great potential in filtration applications, including air filtration, dust capture[12,13] as well as absorbing and detoxifying biological and chemical contaminants.[14,15] We recently demonstrated that polymer nanofibers with polar functional groups such as polyacrylonitrile, polyimide, and nylon-6 have strong affinity to PM pollutants and therefore show high removal efficiency at low pressure drop and high optical transparency.[10,16−18] These nanofibers are promising for use in face masks to achieve both high PM capture efficiency and sufficient air permeability.

On the other hand, thermal comfort of face masks is important and highly desirable, because face masks are used in a wide range of settings, not only by the public to filter polluted air but also by healthcare professionals and sanitation workers in extreme environmental conditions.[11,19,20] It has been found that wearing face masks in hot and humid conditions increases heat stress, sweating, and discomfort.[20] In addition, the moist warm conditions in face masks can act as a breeding ground for micro-organisms, creating an extra exposure hazard to the user.[20] In conventional face masks, the thermal properties (conduction or insulation) are mainly determined by the thickness of the fibers, while the thickness is tightly correlated to the PM removal efficiency (prefers thick fibers) and air permeability (prefers thin fibers). Therefore, it is challenging to manipulate the thermal properties (via changing the thickness of fibers) without sacrificing the other thickness-dependent performances.

Here we demonstrate thermal management in a nanofiber-based face mask with a model system of fiber/nanoPE (nanofibers on nanoporous polyethylene). The nanofibers can effectively remove PM pollutants with low resistance to the air flow. The nanoPE is selected as the supporting substrate because

Received: February 11, 2017
Revised: April 20, 2017

DOI: 10.1021/acs.nanolett.7b00579
Nano Lett. XXXX, XXX, XXX−XXX

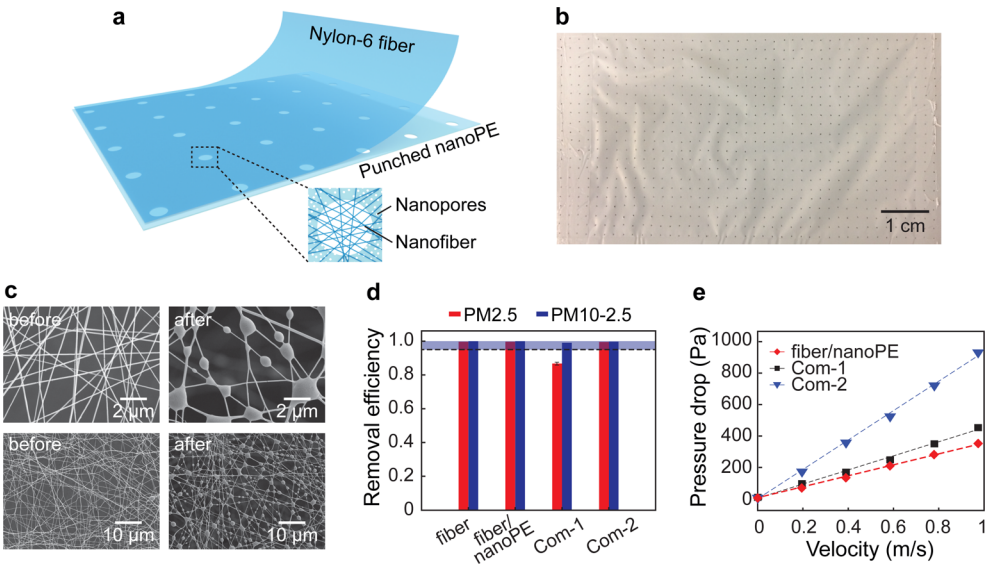

Figure 1. Face mask consisting of nylon-6 nanofibers on top of needle-punched nanoporous-polyethylene (nanoPE) substrate. (a) Scheme for proposed face masks with electrospun nylon-6 nanofibers on needle-punched nanoPE substrate, (b) a photograph of the face mask fiber/nanoPE, (c) SEM images of the nylon-6 fibers before and after filtering the particulate matter (PM), (d) removal efficiency of the fiber/nanoPE compared to two commercial masks, and (e) pressure drop of the fiber/nanoPE and two commercial face masks as a function of the wind velocity.

it is transparent to the mid-infrared (IR) radiation that the human body emits. The design of fiber/nanoPE allows for optimization of filtering performance and thermal properties independently. In high-temperature environment, fiber/nanoPE enables high PM capture efficiency, low pressure drop (ΔP), and excellent radiative cooling properties simultaneously. In low-temperature environment, the nanoPE substrate can be modified by electroless-plating a thin layer of Ag to reflect most of the human body radiation for warming purposes.

Results and Discussion. The design of our proposed face mask, consisting of nylon-6 fibers on a prepunched nanoPE substrate, is shown in Figure 1a. NanoPE is commercially available for use in lithium-ion batteries as a separator with pores of 50−1000 nm in diameter (Figure S1a). Recently, nanoPE has been employed in personal thermal management[21] to reduce energy consumption through enhancing radiative heat dissipation.[22] The nanopores and the micropores punched by microneedles enhance air permeability of the nanoPE (Figure S1b, the needle-punched nanoPE is still abbreviated as nanoPE below). The nylon-6 fibers were fabricated by electrospinning and being transferred onto the nanoPE substrate (Figure S2a, Methods) to enhance their mechanical robustness. Figure 1b shows a typical photograph of the fiber/nanoPE sample. Both the nanoPE substrate (~\$2/m^2) and nylon-6 (~\$0.25/g) are low-cost materials suitable for use in industrial manufacturing. The fibers show good integrity and maintain the morphology after transferred from a roughened Cu substrate to nanoPE (Figure S2b,c).

We first investigated the PM filtering performance of the fiber/nanoPE. The nylon-6 nanofibers with a large range of transmittances (note: the transmittance is used to indicate the fiber density) were prepared to test the PM removal efficiency, which was calculated by comparing the number concentration of the PM particles with and without passing through the fibers (Methods). Our previous work[10,17] has shown that (1) the nanofibers have a higher probability of capturing the PM particles due to larger surface areas compared to large-size fibers at the same packing density, (2) the nanofibers with a large dipole moment of the polymer-repeating unit enhance binding of PM to the polymer surface, and (3) the static charge on nanofibers enables the capturing of PM away from the nanofibers and thus increase the PM capture efficiencies. Therefore, the nylon-6 nanofibers with small fiber diameters (<100 nm) and large dipole moments (3.67D, as compared to 0.6D of polypropylene used in conventional face masks)[10,17] exhibited high removal efficiency (>99.0%) with transmittance up to ~85% (Figure S3a). Besides the removal efficiency, air permeability is another important criterion to assess the performance of filters and can be characterized by the pressure drop (ΔP) across the fibers. As expected, ΔP increases as the transmittance decreases (i.e., increase of fiber density) (Figure S3b). Notably, our nanofibers can simultaneously achieve high PM removal efficiency and low pressure drop at a relatively high transmittance (Figure S3a). In this work, fibers with a transmittance of ~84.5% were used as an example and these nanofibers showed high PM removal efficiency for different PM sizes and under different humidity conditions (Figure S4).

PM particle capture was visualized by the SEM images before and after filtration experiments of the nylon-6 nanofibers (Figure 1c). PM particles with various sizes and morphologies wrapped around the nanofibers and showed strong binding. Both the nylon-6 fiber and fiber/nanoPE exhibited extremely high removal efficiency of 99.9% and 99.6% for $PM_{2.5}$, respectively (Figure 1d). For $PM_{10-2.5}$ with larger particle sizes between 2.5 and 10 μm, both the fiber and fiber/nanoPE showed 99.9% capture efficiencies. The shaded zone (95−100%) in Figure 1d highlights the standard for a high-efficiency mask and both fiber and fiber/nanoPE meet the requirement.

Two commercially available and commonly used face masks (Figure S5, abbreviated as Com-1 and Com-2) were chosen as comparisons, which represent typical masks with different thicknesses and filtering performances. Com-1 had comparable air permeability as fiber/nanoPE (Com-1, ΔP = 450 Pa; fiber/nanoPE, ΔP = 349 Pa at a face velocity of ~1 m/s, Figure 1e) but had much lower efficiency (Com-1, 88.6% for $PM_{2.5}$; fiber/nanoPE, 99.6% for $PM_{2.5}$, Figure 1d). Com-2 had high efficiency

DOI: 10.1021/acs.nanolett.7b00579
Nano Lett. XXXX, XXX, XXX−XXX

(99.8% for $PM_{2.5}$) but the filter layer was much thicker (Com-2, 0.6 mm; as compared to Com-1, 0.08 mm and fiber/nanoPE, 0.012 mm), which resulted in a much higher pressure drop (ΔP = 950 Pa at ~1 m/s, Figure 1e). The overall performance of the face masks considering both removal efficiency and pressure drop is assessed by quality factor[10,16] (QF, Table 1). The fiber/nanoPE exhibited two to three times higher QF than both commercial masks.

Table 1. Quality Factor of the Face Masks[a,b]

sample	E (%)	ΔP (Pa)	QF (Pa^{-1})
fiber/nanoPE	99.6	349	0.0158
Com-1	86.6	450	0.0045
Com-2	99.8	950	0.0065

[a]E (%), capture efficiency; ΔP (Pa), pressure drop. [b]QF = $-\ln(1 - E\%)/\Delta P$ at velocity ~ 1 m/s.

Besides the high PM removal efficiency and low pressure drop, the fiber/nanoPE mask has distinctive functionality of radiative cooling. The human body emits mid-IR radiation centered around 9.5 μm[23] (Figure 2a) which contributes to a large portion of total body heat loss. The objective of thermal management is to enhance/suppress radiative dissipation in the high/low temperature environment.[21,22,24] The total IR transmittance of the samples was measured by a Fourier transform infrared (FTIR) spectrometer equipped with a diffuse gold integrating sphere (Methods). In the range of human body radiation (3−15 μm), polyethylene only had narrow absorption peaks centered around 3.5, 6.8, and 13.9 μm (Figure 2a), which are assigned to CH_2 stretching, bending deformation and rocking deformation, respectively.[25] The weighted average transmittances based on human body radiation were 92.1% for nanoPE, 89.3% for fiber/nanoPE, which were much higher than those of commercial masks (22.9% for Com-1 and 0.5% for Com-2). The large difference in the IR transmittance between fiber/nanoPE and commercial face masks indicates that fiber/nanoPE has a distinct radiative cooling effect by transmitting almost all human body radiation. We tested the face masks and the fiber/nanoPE had high transparency to the human body radiation (Figure 2b), while the commercial face masks blocked a large portion of it. A test on the hot plate showed consistent results (Figure S6).

To further quantify the cooling effect of fiber/nanoPE, we measured the artificial skin temperature with a device that simulated the heat output of skin (Figure 3a). Briefly, a heater was used to simulate the skin with a temperature of 33.5 °C at an ambient temperature of 25 °C. Then the power density of the skin heater and the ambient temperature were both set to be constant. By placing different samples on the simulated skin, a thermocouple in contact with the skin can record the artificial skin temperature (Methods). A guard heater was set to track and generate the same temperature as the artificial skin to avoid downward heat conduction. An insulating polystyrene foam with low thermal conductivity (0.033 W/(m·K)) served the same purpose. The nanoPE and fiber/nanoPE increased the simulated skin temperature by only 1.0 and 0.8 °C, which were much lower than 3.3 and 7.1 °C for Com-1 and Com-2 (Figure 3b). Therefore, the high IR-transparency and excellent heat dissipation capability enabled the superior cooling effect. We also tested the water-vapor transmission and mechanical properties to ensure that the face mask is wearable. The fiber/nanoPE sample had high water vapor transmission rate (~0.018 g/cm^2 hour) that was comparable or even better than the commercial face masks (Figure S7a). In addition, the fiber/nanoPE had decent mechanical robustness compared to the commercial face masks. The mechanical strength can be further reinforced by adding a cotton mesh (Figure S7b).

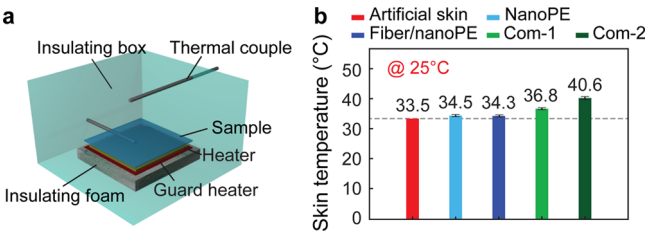

Figure 3. Thermal measurement of the face masks. (a) Experimental setup of the thermal measurement. The heater simulates the skin and the guard heater and insulating foam are used to avoid downward heat loss. The whole device is placed in a temperature-controllable insulating box and two thermal couples record the ambient temperature and the skin temperature, respectively. (b) Skin temperature when covered with different samples: nanoPE, fiber/nanoPE, and two commercial face masks.

Finally, to accommodate the low-temperature environment, a face mask that can reduce the loss of body heat was designed by coating the nanoPE with a layer of Ag via electroless-plating (Methods). Ag-coated nanoPE (Ag/nanoPE) exhibited 95.9% reflectance (weighted by human body radiation) of the IR radiation (Figure 4a). To enhance air permeability, we also needle-punched microholes (~10% in area, Figure S8) on Ag/nanoPE that decreased the reflectance slightly, but both the needle-punched Ag/nanoPE and fiber on needle-punched Ag/nanoPE (abbreviated as fiber/Ag/nanoPE) maintained high

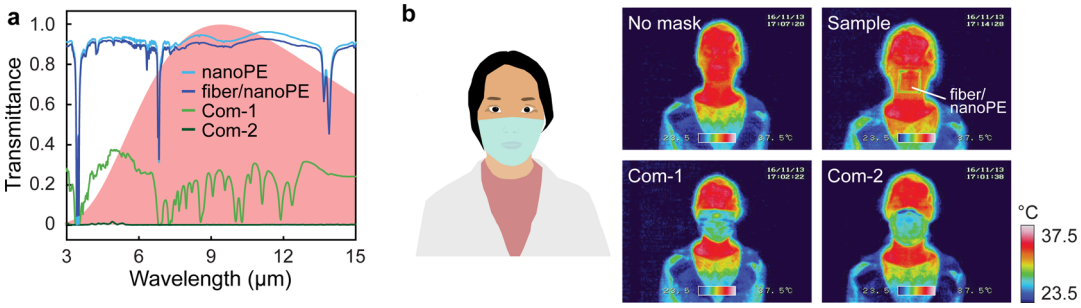

Figure 2. Optical properties and thermal imaging of the face masks. (a) Measured total FTIR transmittance of nanoPE, fiber/nanoPE, and two commercial face masks. The shaded area is the human body radiation. (b) Thermal imaging of bare face and faces covered with the sample (fiber/nanoPE) and two commercial face masks. The rectangular box that appears to be cold was from the tape used to transfer the fibers onto nanoPE.

DOI: 10.1021/acs.nanolett.7b00579
Nano Lett. XXXX, XXX, XXX−XXX

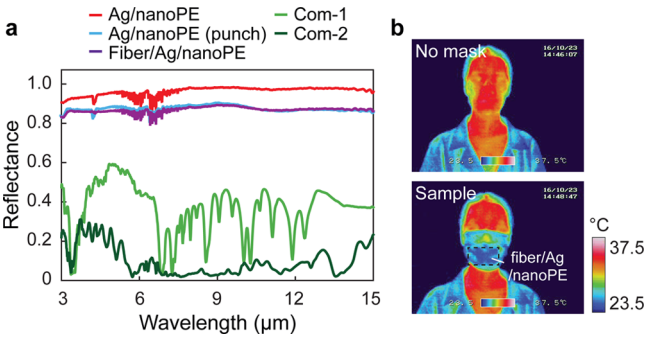

Figure 4. Thermal management of the face mask: optical properties and thermal imaging. (a) Optical reflectance of Ag-coated nanoPE (Ag/nanoPE), needle-punched Ag/nanoPE and fiber/Ag/nanoPE, compared with two commercial face masks. (b) Thermal imaging of the fiber/Ag/nanoPE sample, the layers are arranged from outside to inside as nanofiber, Ag coating, nanoPE, human face.

reflectance (~87.0%, weighted by human body radiation). In contrast, the two commercial face masks only showed 37.8% and 11.1% in reflectance. The thermal image clearly showed that the face covered with fiber/Ag/nanoPE appeared cold because body radiation was blocked from transmission (Figure 4b). The warming effect of the fiber/Ag/nanoPE was tested by measuring how low the ambient temperature could be (i.e., set point) to still maintain the artificial skin temperature (33.5 °C) (Figure 5a,

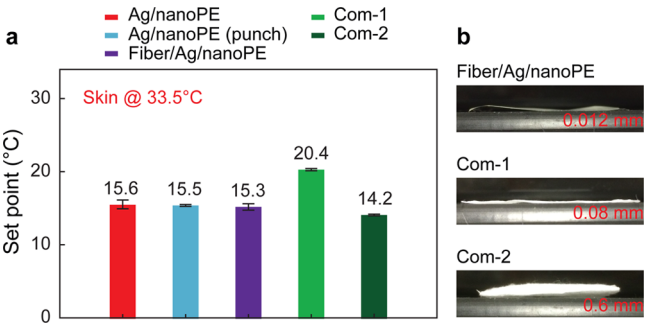

Figure 5. Thermal management of the face mask: thermal measurement. (a) Set point of the ambient temperature to maintain the skin at 33.5 °C, when the skin is covered with different samples. (b) Thickness of the fiber/Ag/nanoPE compared with two commercial masks.

Methods). At the same artificial skin temperature, a lower set point corresponds to higher thermal insulation of the sample. The set point of fiber/Ag/nanoPE was 15.3 °C, comparable to that of Ag-coated nanoPE before and after needle-punching (15.6 and 15.5 °C, respectively). This indicates that fiber/Ag/nanoPE can resist environment temperatures as low as 15.3 °C without affecting personal thermal comfort (i.e., a body-environment temperature difference $\Delta T = 18.2$ °C). In contrast, face mask Com-1 can only resist an environment temperature of 20.4 °C ($\Delta T = 13.1$ °C), even with 7 times the thickness of fiber/Ag/nanoPE (Com-1, 0.08 mm; fiber/Ag/nanoPE, 0.012 mm, Figure 5b). Face mask Com-2 can resist an environment temperature of 14.2 °C ($\Delta T = 19.3$ °C), mainly because of the large thickness (0.6 mm, 50 times that of the fiber/Ag/nanoPE). Thick materials with porosities can have air trapped inside and create insulation to stop outflow of heat, which is a different mechanism for keeping warm that has the disadvantage of bulkiness and low air permeability. Nonetheless, the ultrathin fiber/Ag/nanoPE with high IR reflectance (>85%) and heat insulation properties (Figure S9) provides an excellent candidate for personal thermal management.

Conclusions. In conclusion, we introduce the concept of thermal management into face masks and present a design of fiber/nanoPE that shows high PM capture efficiency, low pressure drop, and excellent radiative cooling effect. We further modify the nanoPE substrate with Ag coating and demonstrate that fiber/Ag/nanoPE has warming effect. These face masks can be used in summer/winter to protect people from polluted air while keeping the user face cool/warm and comfortable. We anticipate face masks with appropriate thermal management will also be useful for indoor applications, for example, in hospitals, to not only filter microorganisms expelled from the mouth and nasopharynx but also to reduce the energy used on indoor cooling/heating because of their effective cooling/warming capabilities.

Methods. *Sample Preparation.* The fiber/nanoPE and fiber/Ag/nanoPE were fabricated by transferring nylon-6 nanofibers onto needle-punched nanoPE or Ag-coated nanoPE substrate. The nylon-6 nanofibers were fabricated by electrospinning. Nylon-6 (Sigma-Aldrich) was dissolved in formic acid (16 wt %), loaded in a 5 mL syringe and pumped out of the needle tip using a syringe pump (KD Scientific). A high voltage (15 kV, ES30P-5W, Gamma High Voltage Research) was applied on the needle tip and a roughened copper foil (Pred Materials) was grounded to collect electrospun nanofibers. The pump rate was 0.06 mL/h. The Ag-coated nanoPE was fabricated by electroless plating of Ag film onto nanoPE. Briefly, the nanoPE was treated by polydopamine (PDA) coating for 2 h in an aqueous solution that consists of 2 g/L dopamine hydrochloride (Sigma-Aldrich) and 10 mM Tris-buffer solution (pH 8.5, Teknova). The PDA-coated nanoPE was then dipped into a 25 g/L $AgNO_3$ solution (99.9%, Alfa Aesar) for 30 min to form a Ag seed layer. Finally, the seeded nanoPE was rinsed with DI water and immersed into the plating bath solution containing 4.2 g/L $Ag(NH_3)_2^+$ (made by adding 28% NH_4OH aqueous solution dropwise into 5g/L $AgNO_3$ until the solution became clear again) and 5 g/L glucose (anhydrous, EMD Millipore Chemicals).

PM Removal Efficiency Measurement. Model PM particles were generated from incense smoke by burning. The smoke PM particles have a wide size distribution from <300 nm to >10 μm, with majority of particles being <1 μm. The inflow concentration was controlled by diluting the smoke by air to a hazardous pollution level equivalent to the PM2.5 index >300. PM particle number concentration was detected with and without face masks by a particle counter (CEM) and the removal efficiency was calculated by comparing the number concentration before and after filtration. The pressure drop was measured by a differential pressure gauge (EM201B, UEi test instrument).

Optical Measurement. The visible transmittance (400−750 nm) was measured by a UV−vis spectrometer (Agilent Cary 6000i UV/vis/NIR). The transmittance spectrum was then weighted by AM1.5 solar spectrum to obtain the average transmittance. The IR transmittance and reflectance were measured by a FTIR spectrometer (Model 6700, Thermo Scientific) accompanied by a diffuse gold integrating sphere (PIKE Technologies).

Thermal Measurement. The skin was simulated by a silicone rubber fiberglass insulated flexible heater (Omega, 72 cm^2) that is connected to a power supply (Keithley 2400). A ribbon type hot junction thermocouple (0.3 mm in diameter, K-type, Omega) was in contact with the top surface of the simulated skin to

DOI: 10.1021/acs.nanolett.7b00579
Nano Lett. XXXX, XXX, XXX−XXX

measure the skin temperature. A guard heater and an insulating foam were placed below the simulated skin heater to ensure that the heat generated by the skin heater only transfer to the ambient. The guard heater was set to track and generate the same temperature as the artificial skin to avoid downward heat conduction and the insulating polystyrene foam with low thermal conductivity (0.033 W/(m·K)) was used for the same purpose. The downward heat losses could make the measured artificial skin temperature (set point) lower (higher) than the real values. The whole device was enclosed in a temperature-controllable chamber. The power density of the skin heater was set to be constant at 73 W/m^2, resulting in a skin temperature of 33.5 °C at the ambient temperature of 25 °C. In the experiments, the skin was covered by the sample and (1) the steady-state ambient temperature needed to maintain the skin temperature at 33.5 °C was recorded as the set point; (2) the temperature of the thermocouple in contact with the simulated skin with constant power density of the skin heater (73 W/m^2) and constant ambient temperature (25 °C) was recorded as the artificial skin temperature. The thermal images were taken by a calibrated thermal camera (MikroSHOT, Mikron).

Water Vapor Transmission Rate Test. This test procedure is based on ASTM E96 with modification. One hundred milliliter media bottles (Fisher Scientific), filled with 60 mL of distilled water, were sealed by the textile samples using open-top caps and silicone gaskets (Corning). The sealed bottles were then placed into an environmental chamber. The temperature and relative humidity inside the chamber were held at 37.5 °C and 30 ± 10%, respectively. The total mass of the bottles together with the samples was measured periodically. The reduced mass, corresponding to the evaporated water, was then divided by the exposed area (3 cm in diameter) to derive the water vapor transmission rate.

Mechanical Test. The tensile strength test was measured by Instron 5565. The textile samples were cut into the shape of 1 cm wide and 5 cm long. The gauge distance was 3 cm long, and the displacement rate was kept at 10 mm/min.

■ ASSOCIATED CONTENT

Supporting Information

The Supporting Information is available free of charge on the ACS Publications website at DOI: 10.1021/acs.nanolett.7b00579.

Characterization of nanoPE and nanofiber. Thermal imaging of fiber/nanoPE and fiber/Ag/nanoPE on hot plate. Water vapor transmission of fiber/nanoPE and fiber/Ag/nanoPE (PDF)

■ AUTHOR INFORMATION

Corresponding Author

*E-mail: yicui@stanford.edu.

ORCID

Ankun Yang: 0000-0002-0274-4025

Hongxia Wang: 0000-0003-0720-3305

Author Contributions

Y.C. and A.Y. designed research. A.Y. and L.C. fabricated Ag-coated nanoPE substrate and performed IR measurement. A.Y. and R.Z. fabricated nanofibers and performed filtration experiments. A.Y. and J.W. performed thermal imaging. P.C.H. set up the thermal measurement. H.W., G.Z., and J.X. helped with research. A.Y. and Y.C. analyzed the data and wrote the paper. All authors discussed the results and commented on the paper.

Notes

The authors declare no competing financial interest.

■ ACKNOWLEDGMENTS

A.Y. acknowledges helpful discussions with Y. Peng, Dr. C. Liu, and Dr. J. Sun.

■ REFERENCES

(1) Seinfeld, J. H.; Pandis, S. N. *Atmospheric Chemistry and Physics: From Air Pollution to Climate Change*; John Wiley & Sons, 2016.
(2) Han, X.; Naeher, L. P. *Environ. Int.* **2006**, *32* (1), 106−120.
(3) Maricq, M. M. *J. Aerosol Sci.* **2007**, *38*, 1079−1118.
(4) Zhang, R.; Jing, J.; Tao, J.; Hsu, S. C. *Atmos. Chem. Phys.* **2013**, *13*, 7053−7074.
(5) Nel, A. *Science* **2005**, *308* (5723), 804−806.
(6) Harrison, R. M.; Yin, J. *Sci. Total Environ.* **2000**, *249* (1−3), 85−101.
(7) Pope, C. A., III; Dockery, D. W. *J. Air Waste Manage. Assoc.* **2006**, *56*, 709−742.
(8) Chow, J. C.; Watson, J. G.; Mauderly, J. L.; Costa, D. L.; Wyzga, R. E.; Vedal, S.; Hidy, G. M.; Altshuler, S. L.; Marrack, D.; Heuss, J. M.; Wolff, G. T.; Arden Pope, C., III; Dockery, D. W. *J. Air Waste Manage. Assoc.* **2006**, *56* (10), 1368−1380.
(9) Zhou, G.; Gan, Y.; Ke, Q.; Knoll, N.; Lonsdale, C.; Schwarzer, R. *Health Psychology* **2016**, *35* (2), 141.
(10) Liu, C.; Hsu, P.-C.; Lee, H.-W.; Ye, M.; Zheng, G.; Liu, N.; Li, W.; Cui, Y. *Nat. Commun.* **2015**, *6*, 6205.
(11) *General Respiratory Protection Guidance for Employers and Workers*; Occupational Safety Health Administration, 2011.
(12) Graham, K.; Ouyang, M.; Raether, T.; Grafe, T. Presented at the *15th Annual Technical Conference & Expo of the American Filtration & Separations Society*; Galveston, Texas; April 9−12, 2002.
(13) Thavasi, V.; Singh, G.; Ramakrishna, S. *Energy Environ. Sci.* **2008**, *1* (2), 205−221.
(14) Ramaseshan, R.; Sundarrajan, S.; Jose, R.; Ramakrishna, S. *J. Appl. Phys.* **2007**, *102* (11), 111101.
(15) Ramaseshan, R.; Sundarrajan, S.; Liu, Y.; Barhate, R. S.; Lala, N. L.; Ramakrishna, S. *Nanotechnology* **2006**, *17* (12), 2947.
(16) Zhang, R.; Liu, C.; Hsu, P.-C.; Zhang, C.; Liu, N.; Zhang, J.; Lee, H. R.; Lu, Y.; Qiu, Y.; Chu, S.; Cui, Y. *Nano Lett.* **2016**, *16*, 3642−3649.
(17) Xu, J.; Liu, C.; Hsu, P.-C.; Liu, K.; Zhang, R.; Liu, Y.; Cui, Y. *Nano Lett.* **2016**, *16*, 1270−1275.
(18) Khalid, B.; Bai, X.; Wei, H.; Huang, Y.; Wu, H.; Cui, Y. *Nano Lett.* **2017**, *17* (2), 1140−1148.
(19) Lipp, A.; Edwards, P. Disposable surgical face masks for preventing surgical wound infection in clean surgery. *Cochrane Database of Systematic Reviews*, 2002, 1, Art. No. CD002929, DOI: 10.1002/14651858.CD002929.
(20) *Respiratory Protective Equipment at Work*; Health and Safety Executive, 2013.
(21) Tong, J. K.; Huang, X.; Boriskina, S. V.; Loomis, J.; Xu, Y.; Chen, G. *ACS Photonics* **2015**, *2* (6), 769−778.
(22) Hsu, P.-C.; Song, A. Y.; Catrysse, P. B.; Liu, C.; Peng, Y.; Xie, J.; Fan, S.; Cui, Y. *Science* **2016**, *353* (6303), 1019−1023.
(23) Sanchez-Marin, F. J.; Calixto-Carrera, S.; Villaseñor-Mora, C. *J. Biomed. Opt.* **2009**, *14* (2), 024006.
(24) Hsu, P.-C.; Liu, X.; Liu, C.; Xie, X.; Lee, H. R.; Welch, A. J.; Zhao, T.; Cui, Y. *Nano Lett.* **2015**, *15*, 365−371.
(25) Gulmine, J. V.; Janissek, P. R.; Heise, H. M.; Akcelrud, L. *Polym. Test.* **2002**, *21* (5), 557−563.

DOI: 10.1021/acs.nanolett.7b00579
Nano Lett. XXXX, XXX, XXX−XXX